A Domain Decomposition Method: A Simulation Study

Carlo Cercignani[1], Irene M. Gamba[2], Joseph W. Jerome[3], and Chi-Wang Shu[4]

[1]Politecnico di Milano, 20133 Milano, Italy

[2]University of Texas, Austin, TX 78712, USA

[3]Northwestern University, Evanston, IL 60208, USA
E-mail: jwj@math.nwu.edu

[4] Brown University, Providence, RI 02912, USA

1. Introduction

In previous work [2], the authors introduced a conceptual domain decomposition approach, combining drift-diffusion, kinetic, and high-field regimes. The high-field model had been introduced in [4]. The approach was implemented in preliminary form in [3]. In this paper, we continue the program begun in [2]. We again define a global calibrator, a linear approximation to the Boltzmann transport equation, and solve this in one space and one velocity dimension.

Second, we implement a global domain decomposition method, by systematic sampling of separation points between drift-diffusion and high field regimes. The interdomain boundary conditions are implemented through the stencil overlap of the algorithms in both regions.

2. Models Employed

Kinetic Model

The one-dimensional kinetic model can be written as follows:

$$\frac{\partial f(x,u,t)}{\partial t} + u\frac{\partial f(x,u,t)}{\partial x} - \frac{e}{m}E(x,t)\frac{\partial f(x,u,t)}{\partial u} = \frac{n(x,t)M(u) - f(x,u,t)}{\tau}, \tag{1}$$

where

$$M(u) = \frac{1}{\sqrt{2\pi\theta}}e^{-\frac{u^2}{2\theta}} \tag{2}$$

is a Maxwellian, with

$$\theta = \frac{k_b}{m}T_0. \tag{3}$$

The concentration $n(x,t)$ is obtained by

$$n(x,t) = \int_{-\infty}^{\infty} f(x,u,t)du. \tag{4}$$

Also, the electric field $E(x,t)$ is obtained by solving the coupled potential equation,

$$E(x,t) = -\phi_x, \qquad (\epsilon\phi_x)_x = e(n - n_d), \tag{5}$$

with the boundary conditions

$$\phi(0,t) = 0, \qquad \phi(0.8,t) = vbias, \tag{6}$$

and the relaxation parameter τ is computed by

$$\tau = \frac{m\mu}{e}. \tag{7}$$

μ is the mobility. In this paper we use a variable μ depending on the electric field E, used in drift-diffusion simulations to model saturation (see [5]):

$$\mu(E) = 2\mu_0 / \left[1 + \sqrt{1 + 4(\mu_0|E|/v_d)^2}\right], \tag{8}$$

where

$$\mu_0 = 4.0\ \mu m^2/(V\,ps), \qquad v_d = 2.0\ \mu m/ps. \tag{9}$$

v_d here is taken to be the maximum of the velocity in the kinetic run with $vbias = 1.0$ and $\mu = 4$.

The Drift-Diffusion (DD) Model

The drift-diffusion (DD) model is well documented (see, for example, [5]). It is given by:

$$n_t + J_x = 0, \tag{10}$$

where

$$J = J_{hyp} + J_{vis},$$

and

$$J_{hyp} = -\mu n E,$$
$$J_{vis} = -\tau(n\theta)_x.$$

0-7803-4369-7/98 $10.00

The High-Field (HF) Model

The model can be written as follows:

$$n_t + J_x = 0, \tag{11}$$

where

$$J = J_{hyp} + J_{vis},$$

and

$$J_{hyp} = -\mu n E + \tau\mu \left(\frac{e}{\epsilon}\right) n(-\mu n E + \omega),$$

$$J_{vis} = -\tau[n(\theta + 2\mu^2 E^2)]_x + \tau\mu E(\mu n E)_x.$$

For our current one dimensional case, ω is taken to be a constant:

$$\omega = (\mu n E)|_{x=0}.$$

It is developed in [4] by asymptotic expansion methods (Chapman-Enskog) for the kinetic formulation of the problem (1)–(5), under strong forcing scaling assumptions.

Other augmented drift-diffusion models are found in [7,8].

3. Simulation Description

The device we consider for this paper is the one dimensional GaAs n^+-n-n^+ structure of length $0.8\mu m$. The device used is as follows: $x \in [0, 0.8]$; the doping is defined by $n_d(x) = 10^6/\mu m^3$ in $0 \le x \le 0.175$ and in $0.625 \le x \le 0.8$, and by $n_d(x) = 2 \times 10^3/\mu m^3$ in $0.225 \le x \le 0.575$, with a smooth intermediate transition. This is exactly the device used in Baranger and Wilkins [1], except for a smooth transition of width $0.05\mu m$ at the junctions.

More specific conditions for various models are listed below.

(I) For the kinetic model (1):

(a) The velocity space is artificially cut at

$$-a \le u \le a \tag{12}$$

where we monitor to ensure that $f(x, u, t)$ is always very small at the boundary $u = \pm a$ for the final steady state results. We learned that it is more than enough in all our runs to use $a = 3.5$. Larger values of a are also used to verify that the results do not change in the pictures.

(b) We use a uniform grid both in x and in u, with 160×150 points. A more refined mesh is also used to verify that the results do not change in the pictures.

(c) At $x = 0$, take

$$f(0, u, t) \;=\; n_d(0)\, M(u) \tag{13}$$

if $u \ge 0$, and no boundary condition (extrapolation of the numerical solution from inside the domain to the boundary) if $u < 0$. Also take $\phi(0, t) = 0$.

(d) At $x = 0.8$, take

$$f(0.8, u, t) \;=\; n_d(0.8)\, M(u) \tag{14}$$

if $u \le 0$, and no boundary condition (extrapolation of the numerical solution from inside the domain to the boundary) if $u > 0$. Also take $\phi(0, t) = vbias$.

(e) At $u = -a$ and $u = a$, take no boundary condition (extrapolation of the numerical solution from inside the domain to the boundary).

(II) For the elementary domain decomposition, we apply the low field drift-diffusion (DD) model (10) in [0,A] and [B,0.8], and the high-field (HF) model (11) in (A,B). We experiment with the separation locations A, B with a systematic sampling. For each fixed pair (A,B), we perform the following:

(a) We use a uniform grid in x with 160 points.

(b) At $x = 0$ and $x = 0.8$, take the boundary conditions

$$n(0, t) = n_d(0), \phi(0, t) = 0,$$

$$n(0.8, t) = n_d(0.8), \phi(0.8, t) = vbias.$$

(c) At the interfaces $x = A$ and $x = B$, there are no explicit interface boundary conditions. The coupling of the drift-diffusion model and the high field model is through the ghost points used in the computation:

(i) When a grid point is inside [0,A] or [B,0.8], the solution n is updated by the drift-diffusion model (10) using a fifth order conservative WENO scheme (see [6]). Since this scheme has a 7-point stencil, when computing the updates near the interfaces A or B, the stencil actually goes into the region (A,B), hence the information in that high field region is used.

(ii) Similarly, the high field model (11) is used to update the solution if the grid point is inside (A,B). Again, the 7-point stencil of the numerical scheme implies that information inside the drift-diffusion region [0,A] and [B,0.8] is used when the grid point is near the interfaces A and B.

Simulations are performed for *vbias* from 0V to 2V, and results are shown for selected cases to save space. Other parameters: $m = 0.065 \times 0.9109$ $(10^{-30} Kg)$, $e = 0.1602$ $(10^{-18} C)$, $k_b = 0.138046 \times 10^{-4}$ $(10^{-18} J/Kelvin)$, $\epsilon = 13.2 \times 8.85418$ $(10^{-18} F/\mu m)$.

4. Simulation Results

In all the numerical simulations, we perform a long time integration until a steady state is reached. We perform a preliminary domain decomposition in the channel region alone, to motivate the elementary domain decomposition to follow. This highlights the effectiveness of the high field model in the channel region. Thus, in Figure 1, we plot the comparison among the mid-region simulations of DD and HF, and the global kinetic simulation, for the concentration n, at $vbias = 1$V. We perform the mid-region simulation for HF and DD with the boundary conditions provided by the kinetic simulation using $\mu = \mu(E)$ given by (8). We can see that the high-field model has a much better agreement with the kinetic simulations.

We perform the elementary domain decomposition by applying the low field drift diffusion model in [0,A] and [B,0.8], and the high field model in (A,B). Given the concentration n at the time level k, for points within [0,A]

and [B,0.8], the update to the next time level is via the low field drift diffusion model. For points within (A,B), the update to the next time level is via the high field model. Interface coupling is implicit through the 7-point stencil of WENO schemes used for both models, as explained before.

For $vbias = 1V$ and $vbias = 1.8V$, we perform a systematic sampling to find a good pair (A,B). The results are shown in Figures 2 to 4 for $vbias = 1V$, $A = 0.27$ and $B = 0.55$, and in Figures 5 to 7 for $vbias = 1.8V$, $A = 0.25$ and $B = 0.55$.

References

1. H. U. Barenger and J. W. Wilkins: Phys. Rev. B **36** (1987) 1487.

2. C. Cercignani, I. M. Gamba, J. W. Jerome and C-W. Shu: VLSI DESIGN **8** (1998) 135.

3. C. Cercignani, I. M. Gamba, J. W. Jerome and C-W. Shu: VLSI DESIGN **8** (1998) 275.

4. C. Cercignani, I. M. Gamba and C. D. Levermore: Appl. Math. Lett. **10** (1997) 111.

5. J. W. Jerome: *Analysis of Charge Transport: A Mathematical Study of Semiconductor Devices* (Springer, 1996).

6. G. Jiang and C.-W. Shu: J. Comput. Phys. **126** (1996) 202.

7. E. C. Kan, U. Ravaioli and T. Kerkhoven: Solid-State Electr. **34** (1991) 995.

8. K. K. Thornber: IEEE Electron Device Lett. **3** (1983) 69.

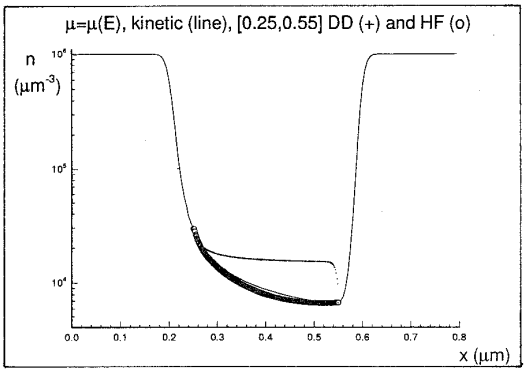

Figure 1: The global kinetic simulation (solid line), the mid-region HF simulation (circles), and the mid-region DD simulation (plus signs). $\mu = \mu(E)$ for all simulations. The global kinetic simulation provides the boundary conditions for the mid-region HF and DD simulations. The concentration n in μm^{-3}.

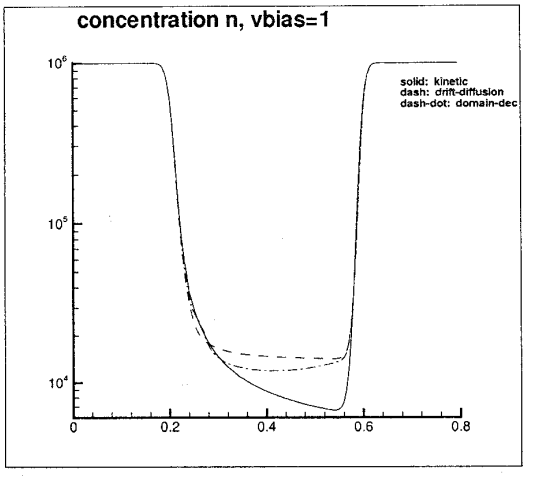

Figure 2: The concentration n. $\mu = \mu(E)$. $vbias = 1V$. Comparison among the kinetic result (solid line), the low field drift-diffusion model (dashed line), and the elementary domain decomposition with low field drift-diffusion in [0,0.27] and [0.55,0.8], and high field model in (0.27,0.55) (dash-dotted line).

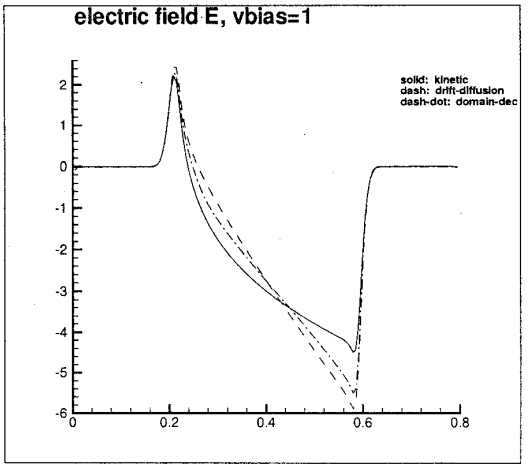

Figure 3: The electric field E. $\mu = \mu(E)$. $vbias = 1V$. Comparison among the kinetic result (solid line), the low field drift-diffusion model (dashed line), and the elementary domain decomposition with low field drift-diffusion in [0,0.27] and [0.55,0.8], and high field model in (0.27,0.55) (dash-dotted line).

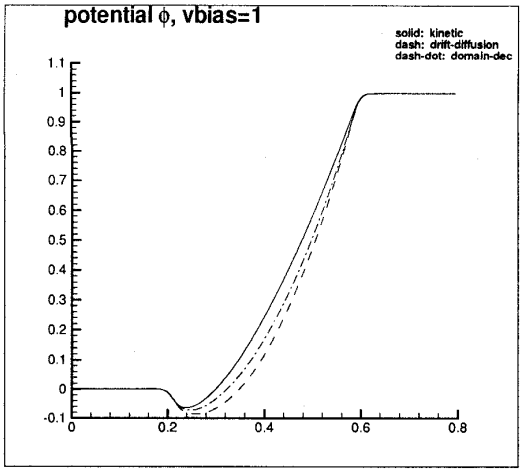

Figure 4: The potential ϕ. $\mu = \mu(E)$. $vbias = 1V$. Comparison among the kinetic result (solid line), the low field drift-diffusion model (dashed line), and the elementary domain decomposition with low field drift-diffusion in [0,0.27] and [0.55,0.8], and high field model in (0.27,0.55) (dash-dotted line).

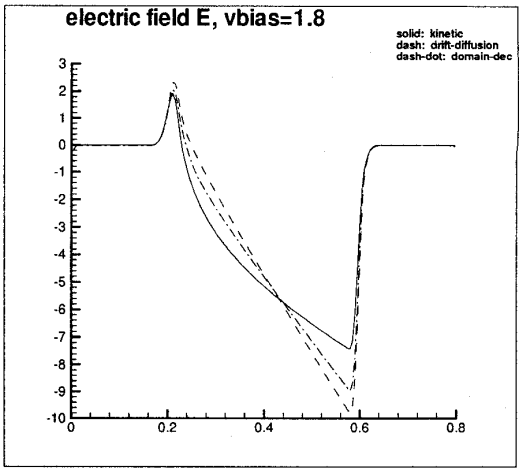

Figure 6: The electric field E. $\mu = \mu(E)$. $vbias = 1.8V$. Comparison among the kinetic result (solid line), the low field drift-diffusion model (dashed line), and the elementary domain decomposition with low field drift-diffusion in [0,0.25] and [0.55,0.8], and high field model in (0.25,0.55) (dash-dotted line).

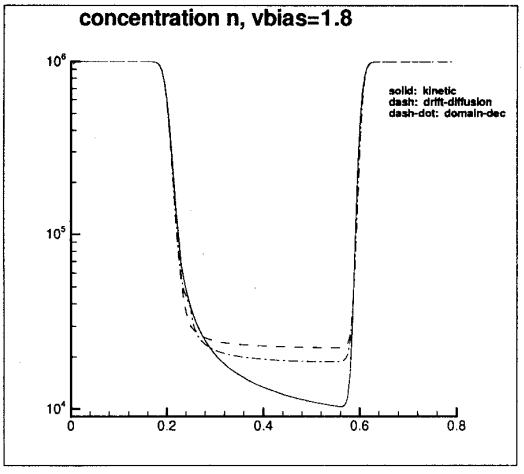

Figure 5: The concentration n. $\mu = \mu(E)$. $vbias = 1.8V$. Comparison among the kinetic result (solid line), the low field drift-diffusion model (dashed line), and the elementary domain decomposition with low field drift-diffusion in [0,0.25] and [0.55,0.8], and high field model in (0.25,0.55) (dash-dotted line).

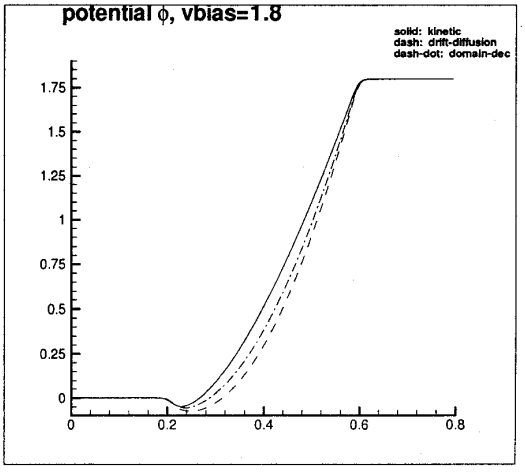

Figure 7: The potential ϕ. $\mu = \mu(E)$. $vbias = 1.8V$. Comparison among the kinetic result (solid line), the low field drift-diffusion model (dashed line), and the elementary domain decomposition with low field drift-diffusion in [0,0.25] and [0.55,0.8], and high field model in (0.25,0.55) (dash-dotted line).